Optimized Tersoff and Brenner empirical potential parameters for lattice dynamics and phonon thermal transport in carbon nanotubes and graphene

L. Lindsay
Department of Physics, Boston College, Chestnut Hill, Massachusetts 02467, USA
and Department of Physics, Computer Science, and Engineering, Christopher Newport University, Newport News, Virginia 23606, USA

D. A. Broido
Department of Physics, Boston College, Chestnut Hill, Massachusetts 02467, USA
(Received 3 March 2010; revised manuscript received 10 May 2010; published 27 May 2010)

We have examined the commonly used Tersoff and Brenner empirical interatomic potentials in the context of the phonon dispersions in graphene. We have found a parameter set for each empirical potential that provides improved fits to some structural data and to the in-plane phonon-dispersion data for graphite. These optimized parameter sets yield values of the acoustic-phonon velocities that are in better agreement with measured data. They also provide lattice thermal conductivity values in single-walled carbon nanotubes and graphene that are considerably improved compared to those obtained from the original parameter sets.

DOI: 10.1103/PhysRevB.81.205441 PACS number(s): 63.22.Rc, 65.80.−g, 63.20.−e, 65.40.−b

I. INTRODUCTION

It is well known that carbon-based materials such as diamond, graphite, graphene, and carbon nanotubes possess the highest known thermal conductivities.[1–9] This has motivated intense theoretical effort to understand the thermal transport properties of these systems.[10–30] Such investigations commonly employ either molecular-dynamics simulations or Boltzmann transport equation (BTE) approaches. In both cases accurate representation of the interactions between atoms is required. Harmonic interatomic force constants (IFCs) are required to obtain phonon frequencies and eigenvectors, and acoustic-phonon velocities. Real-space anharmonic IFCs are also needed to describe the phonon-phonon scattering that is responsible for the intrinsic thermal resistance.

Rigorous first-principles and force-constant approaches have been employed in graphene and single-walled carbon nanotubes (SWCNTs) to calculate the harmonic IFCs in these systems, and highly accurate phonon dispersions have been obtained over the entire Brillouin zone.[31–33] Anharmonic IFCs have also been obtained recently in these systems using density-functional perturbation theory (DFPT) and used successfully in phonon lifetime calculations.[34,35] However, DFPT calculations of the real-space anharmonic IFCs are considerably more difficult so no commonly available *ab initio* DFPT package, such as QUANTUM ESPRESSO,[36] VASP,[37] and ABINIT (Ref. 38) generates them. In contrast, empirical interatomic potentials (EIPs) provide these anharmonic interactions in a conveniently extractable form and so are frequently used in thermal transport calculations in SWCNTs and more recently in graphene.[23,24,30] The most commonly used EIPs are those developed by Tersoff[39,40] and Brenner.[41,42]

The Tersoff and Brenner EIPs are short range and so cannot accurately fit the graphene dispersion over the entire Brillouin zone. However, the thermal conductivity depends more sensitively on the accuracy of acoustic phonon frequencies near the zone center where the longitudinal- and transverse-acoustic (LA and TA) velocities and the quadratic curvature of the out-of-plane acoustic (ZA) branch are determined. On the other hand, only weak thermal excitation of the optic phonons and acoustic phonons near the Brillouin-zone boundary occurs around room temperature because of the large graphene Debye temperature (~2000 K). Therefore, accurate fitting to the corresponding phonon frequencies is less important.

The original parameter sets of the Tersoff and Brenner EIPs do not accurately reproduce the phonon dispersions of graphene, as has been noted previously.[43] In particular, they do not accurately obtain the velocities of the three acoustic branches near the center of the Brillouin zone, thus, also misrepresenting these properties in SWCNTs. We present here optimized parameter sets for the Tersoff and Brenner EIPs, which better represent the lattice dynamical properties of graphene. We test these optimized parameter sets on the lattice thermal conductivities of SWCNTs and graphene, and we find them to yield values that are in much better agreement with available data. In Sec. II we briefly describe the Tersoff and Brenner EIPs and the approach we took in optimizing the empirical parameters. Section III presents the optimized parameter sets and compares the graphene phonon dispersions obtained from the original and optimized parameter sets. It also examines the phonon thermal conductivities of SWCNTs and graphene obtained from old and new parameter sets for both EIPs. Section IV presents a summary and conclusions.

II. THEORY

The convenience of the Tersoff and Brenner EIPs comes from their rather simple, analytical forms and the short range of atomic interactions. For carbon-based systems, the Tersoff model has nine adjustable parameters (listed in Table I) that were originally fit to cohesive energies of various carbon systems, the lattice constant of diamond, and the bulk modulus of diamond. The Brenner EIP is based directly on the Tersoff EIP but has additional terms and parameters which

TABLE I. Original parameters for the Tersoff EIP for carbon-based systems given in Ref. 40.

$A=1393.6$ eV	$B=346.74$ eV
$\lambda_1=3.4879$ Å^{-1}	$\lambda_2=2.2119$ Å^{-1}
$\lambda_3=0.0000$ Å^{-1}	$n=0.72751$
$c=38049.0$	$\beta=1.5724\times10^{-7}$
$d=4.3484$	$h=-0.57058$
$R=1.95$ Å	$D=0.15$ Å

allow it to better describe various chemical reactions in hydrocarbons and include nonlocal effects (parameters listed in Table II).

A. Tersoff model

The analytical form for the pair potential, V_{ij}, of the Tersoff model is given by the following functions with corresponding parameters listed in Table I:[39,40]

$$V_{ij}=f_{ij}^{C}(a_{ij}f_{ij}^{R}-b_{ij}f_{ij}^{A}), \tag{1a}$$

$$f_{ij}^{R}=Ae^{-\lambda_1 r_{ij}}, \tag{1b}$$

$$f_{ij}^{A}=Be^{-\lambda_2 r_{ij}}, \tag{1c}$$

where r_{ij} is the distance between atoms i and j, f_{ij}^{A} and f_{ij}^{R} are competing attractive and repulsive pairwise terms, and f_{ij}^{C} is a cutoff term which ensures only nearest-neighbor interactions. The term, a_{ij}, is a range-limiting term on the repulsive potential that is typically set equal to 1. We do so here. The bond angle term, b_{ij}, depends on the local coordination of atoms around atom i and the angle between atoms i, j, and k,

$$b_{ij}=(1+\beta^n\zeta_{ij}^n)^{-1/2n}, \tag{2a}$$

$$\zeta_{ij}=\sum_{k\neq i,j}f_{ik}^{C}g_{ijk}e^{\lambda_3^3(r_{ij}-r_{ik})^3}, \tag{2b}$$

TABLE II. Original parameters for the Brenner EIP for solid-state carbon-based structures given in Ref. 42. Also listed are the coefficients for the fifth-order polynomial spline, g_{ijk}, described in Ref. 42.

$A=10953.544162170$ eV	$B_1=12388.79197798$ eV
$B_2=17.56740646509$ eV	$B_3=30.71493208065$ eV
$\alpha=4.7465390606595$ Å^{-1}	$\lambda_1=4.7204523127$ Å^{-1}
$\lambda_2=1.4332132499$ Å^{-1}	$\lambda_3=1.3826912506$ Å^{-1}
$Q=0.3134602960833$ Å	$R=2.0$ Å
$D=1.7$ Å	$T_0=-0.00809675$
$\beta_0=0.7073$	$\beta_1=5.6774$
$\beta_2=24.0970$	$\beta_3=57.5918$
$\beta_4=71.8829$	$\beta_5=36.2789$

$$g_{ijk}=1+\frac{c^2}{d^2}-\frac{c^2}{d^2+(h-\cos[\theta_{ijk}])^2}, \tag{2c}$$

where θ_{ijk} is the angle between atoms i, j, and k. This bond angle term allows the Tersoff model to describe the strong covalent bonding that occurs in carbon systems, which cannot be represented by purely central potentials. This angle-dependent term also allows for description of carbon systems that bond in different geometries, such as tetrahedrally bonded diamond and the 120° tribonded graphene.

B. Brenner model

The Brenner potential for solid-state carbon structures is given by the following functions with corresponding parameters listed in Table II:[41,42]

$$V_{ij}=f_{ij}^{C}(f_{ij}^{R}-\bar{b}_{ij}f_{ij}^{A}), \tag{3a}$$

$$f_{ij}^{R}=\left(1+\frac{Q}{r_{ij}}\right)Ae^{-\alpha r_{ij}}, \tag{3b}$$

$$f_{ij}^{A}=\sum_{n=1}^{3}B_n e^{-\lambda_n r_{ij}}, \tag{3c}$$

where many of the terms are similar to the Tersoff model described above and the bond angle term, $\bar{b}_{ij}$, is given by

$$\bar{b}_{ij}=\frac{1}{2}(b_{ij}^{\sigma-\pi}+b_{ji}^{\sigma-\pi})+\Pi_{ij}^{RC}+b_{ij}^{DH}, \tag{4a}$$

$$b_{ij}^{\sigma-\pi}=\left(1+\sum_{k\neq i,j}f_{ik}^{C}g_{ijk}\right)^{-1/2}, \tag{4b}$$

$$g_{ijk}=\sum_{i=0}^{5}\beta_i\cos^i[\theta_{ijk}]. \tag{4c}$$

Here, $b_{ij}^{\sigma-\pi}$ depends on the local coordination of atoms around atom i and the angle between atoms i, j, and k, θ_{ijk}. This pi-bond function is symmetric for graphene, graphite, and diamond, $b_{ij}^{\sigma-\pi}=b_{ji}^{\sigma-\pi}$. The coefficients, β_i, in the bond-bending spline function, g_{ijk}, were fit to experimental data for graphite and diamond and are also listed in Table II. The term, Π_{ij}^{RC}, accounts for various radical energetics, such as vacancies, which are not considered here; thus, this term is taken to be zero. The term, b_{ij}^{DH}, is a dihedral bending function that depends on the local conjugation and is zero for diamond but important for describing graphene and SWCNTs. This dihedral function involves third-nearest-neighbor atoms and is given by[41,42,44]

$$b_{ij}^{DH}=\frac{T_0}{2}\sum_{k,l\neq i,j}f_{ik}^{C}f_{jl}^{C}(1-\cos^2[\Theta_{ijkl}]), \tag{5}$$

where T_0 is a parameter, f_{ij}^{C} is the cutoff function, and Θ_{ijkl} is the dihedral angle of four atoms identified by the indices, i, j, k, and l, and is given by

$$\cos[\Theta_{ijkl}] = \vec{\eta}_{jik} \cdot \vec{\eta}_{ijl}, \tag{6a}$$

$$\vec{\eta}_{jik} = \frac{\vec{r}_{ji} \times \vec{r}_{ik}}{|\vec{r}_{ji}||\vec{r}_{ik}|\sin[\theta_{ijk}]}, \tag{6b}$$

where $\vec{\eta}_{jik}$ and $\vec{\eta}_{ijl}$ are unit vectors normal to the triangles formed by the atoms given by the subscripts, $\vec{r}_{ij}$ is the vector from atom i to atom j, and θ_{ijk} is the angle between atoms i, j, and k. In flat graphene, the dihedral angle, Θ_{ijkl}, is either 0 or π and the dihedral term is subsequently zero.[44] Bending of the graphene layer leads to a contribution from this term.

Some of the main differences when compared to the Tersoff EIP are: the Brenner EIP includes two additional exponential terms with corresponding adjustable parameters in the attractive pairwise term, it includes a screened Coulomb term in the repulsive pairwise term, it uses a fifth-order polynomial spline between bond orders for diamond and graphite, and it includes a dihedral bending term for bond energies which plays a role in SWCNTs and graphene.

C. Parameter optimization

We have implemented a χ^2 minimization procedure for each of these EIPs. A numerical algorithm was developed to minimize χ^2 given by[45,46]

$$\chi^2 = \sum_i \frac{(\eta_i - \eta_{\text{exp}})^2}{\eta_{\text{exp}}^2} \zeta_i, \tag{7}$$

where η_{exp} are experimental parameters used in the fitting process, η_i are the corresponding values obtained using each potential, and ζ_i are weighting factors that determine the relative importance of η_i in the fitting procedure.

In minimizing χ^2, the greatest significance was given to the phonon frequencies, ω_λ, and the zone-center acoustic velocities, $\bar{v}_\lambda = d\omega_\lambda / d\vec{q}$, of graphene in the high-symmetry directions. Here, $\lambda = (\vec{q}, j)$ designates a phonon with wave vector, $\vec{q}$, in branch, j. The phonon frequencies are determined by diagonalization of the dynamical matrix for a given $\vec{q}$ in the two-dimensional graphene Brillouin zone. The dynamical matrix is

$$D_{\alpha\beta}^{\kappa\kappa'}(\vec{q}) = \frac{1}{\sqrt{m_\kappa m_{\kappa'}}} \sum_{\ell'} \Phi_{\alpha\beta}^{0\kappa,\ell'\kappa'} e^{i\vec{q}\cdot\vec{R}_{\ell'}}, \tag{8}$$

where $\ell\kappa$ designates the κth atom in the ℓth unit cell, m_κ is the mass of the κth atom, $\vec{R}_\ell$ is the lattice vector for the ℓth unit cell, and α and β are Cartesian components. In Eq. (8), $\Phi_{\alpha\beta}^{0\kappa,\ell'\kappa'}$ are second-order IFCs which are determined by each EIP.

We attached the most significance to the phonon frequencies and zone-center acoustic velocities because of the important roles that they play in thermal transport calculations. The parameters calculated by each EIP for graphene were compared to the corresponding experimental parameters for in-plane graphite. First-principles calculations of the phonon dispersions in graphene have found excellent agreement with measured in-plane dispersion of graphite.[31,32] This is consistent with the known weak coupling between the graphene layers in graphite. The cohesive energies and lattice constants of graphite and diamond were also considered in the minimization procedure but were given lesser weight.

Using this minimization procedure for the Tersoff EIP, we found that simply modifying the h parameter, which helps to adjust the strength of the bond-angle term, provided vast improvement to the optical branches of the phonon dispersion, while also improving the fit to the TA zone-center velocity. Adjustment of the B parameter associated with the strength of the attractive term was required to retain a decent fit to the experimental lattice constants for both graphite and diamond. Simple adjustment of the h parameter has previously been found to significantly improve the fits to the measured linear expansion coefficient[47] and thermal conductivity of bulk silicon.[48]

A slightly different approach was taken in optimizing the Brenner model to better fit the phonon spectrum. The Brenner potential includes a dihedral bonding term, not included in the Tersoff model, which plays a role in graphene systems. The dihedral term, Eq. (5), has a single adjustable parameter, T_0, which was determined by fitting the lattice constant of a hypothetical three-dimensional, hexagonal system whose dihedral bond angles are $\pi/2$.[42,49] Changing this parameter alone simply alters the out-of-plane acoustic and optic (ZA and ZO) modes in graphite but leaves the other phonon modes unaltered and has no effect on diamond since T_0 is zero for the tetrahedral configuration. We have chosen to adjust this parameter to better fit the phonon frequencies for the ZA branch in graphite.

The six coefficients, β_i, in the fifth-order polynomial spline, g_{ijk}, [Eq. (4c)] used to represent the bond-bending term in the Brenner EIP introduce additional flexibility not available in the Tersoff potential. These coefficients were originally determined by fixing the values of the g_{ijk} and their first and second derivatives at 109° and 120° (corresponding to diamond and graphite bond angles) to match various experimental data.[42] The values for g_{ijk} were determined by fitting the cohesive bond energies of graphite and diamond while the second derivatives were chosen to fit the elastic constants, c_{11}, for diamond and in-plane graphite. The first derivatives were simply chosen to suppress oscillations of the spline function. The coefficients, β_i, are determined from these values for g_{ijk}. These coefficients fix the spline and its derivatives at the bond angles for diamond and graphite, and the function is interpolated between these angles. Thus, they can be adjusted to separately fit experimental data for graphite while leaving the representation for diamond unaltered. The bond angles for SWCNTs, though close to graphite, fall between these two structures and thus depend on both. We note that the bond angles for large diameter SWCNTs approach that of graphite.

We restricted the parameter optimization of the Brenner potential to T_0 and β_i to avoid significantly altering the previous fits to the extensive structural experimental data sets.[41,42] The values for g_{ijk} at 109° and 120° were altered slightly to better fit the given experimental lattice constants for diamond and graphite. We then adjusted the values of the second derivatives of g_{ijk} in these materials to better fit the zone-center acoustic velocities and corresponding phonon frequencies. Upon plotting the fifth-order polynomial spline

TABLE III. Optimized parameters and coefficients for the Tersoff and Brenner EIPs. All parameters not listed are unaltered from the original sets.

Tersoff	
$h=-0.930$	$B=430.0$ eV
Brenner	
$T_0=-0.0165$	
$\beta_0=0.0000$	$\beta_1=-3.1822$
$\beta_2=-19.9928$	$\beta_3=-51.4108$
$\beta_4=-61.9925$	$\beta_5=-29.0523$

given by the old coefficients versus the optimized coefficients no visual difference can be seen. However, these small changes introduce noticeable changes in the corresponding phonon dispersions in graphene.

III. RESULTS AND DISCUSSION

The optimized parameter sets for the Tersoff and Brenner EIPs are listed in Table III. These parameters provide improved fits to experimental phonon-acoustic velocities and frequencies without significantly altering fits to other structural data. The calculated phonon dispersion for graphene as given by the Tersoff (Brenner) EIP is shown in Fig. 1 (Fig. 2) along with the corresponding measured in-plane phonon dispersion for graphite.[50,51] In each figure the black (red) lines correspond to the optimized (original) parameter sets.

The original set of parameters for the Tersoff EIP gives higher values for the TA branch velocities in the high-symmetry directions compared to the measured data while giving values for the quadratic ZA frequencies that fall below experiment around the M point. The most obvious failure of the Tersoff EIP in describing the phonon dispersion of

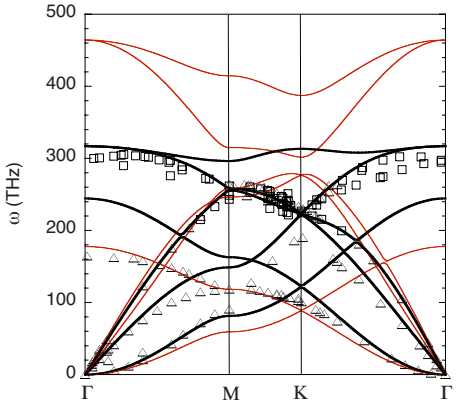

FIG. 1. (Color online) Phonon dispersion for graphene along high-symmetry directions obtained using the Tersoff EIP. Thick black lines correspond to the optimized parameter set (this work); thin red lines correspond to the original parameter set. Squares (triangles) are in-plane experimental data points for graphite from Ref. 43 (Ref. 44).

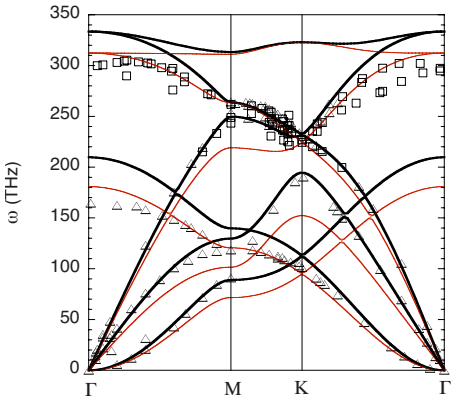

FIG. 2. (Color online) Phonon dispersion for graphene as given by the Brenner EIP for high-symmetry directions. Thick black lines correspond to the optimized parameter set (this work); thin red lines correspond to the original parameter set. Squares (triangles) are in-plane experimental data points for graphite from Ref. 43 (Ref. 44).

graphene comes in the highest optical branches, as seen in Fig. 1. The measured in-plane upper optic modes at the Γ point are degenerate with a value of 300 THz, while the Tersoff potential gives a value of 470 THz, a discrepancy of nearly 40%. The Tersoff model using the optimized parameter set more accurately describes these upper optic phonon branches while providing a decent fit to the acoustic velocities and phonon frequencies. However, using these parameters provides a poorer fit to the experimental dispersion for the out-of-plane ZO branch. The inability to simultaneously fit the acoustic branches and all of the optic branches is a consequence of the Tersoff potential's short range with only second-nearest-neighbor interactions represented. Tewary and Yang[43] obtained a better fit to the phonon dispersion in graphene using a longer-range EIP that extended to fourth-nearest neighbors. Los *et al.*[52] have also developed a somewhat more complicated long-range EIP based on the Brenner EIP, though, phonon dispersion results have not yet been published.

The original set of Brenner parameters, while providing a much better description of the optic branches, does not accurately represent the zone-center velocities for all of the acoustic modes. With the original Brenner EIP parameters, the velocities of the TA branch in the high-symmetry directions are too low by 30%, those of the LA branch 12% too small, and the dispersion of the ZA branch undershoots the data by as much as 20%. The optimized parameter set improves the fit to the zone-center acoustic velocities and most of the experimental ZA, TA, and LA dispersion data. This optimized set provides a somewhat worse fit to the optic dispersion. The inability to simultaneously fit both acoustic and optic branches is again most likely a consequence of the short range of this EIP.

Table IV lists measured lattice constants, cohesive energies, and acoustic velocities in the $\Gamma \rightarrow M$ direction for graphite and the $\Gamma \rightarrow X$ direction for diamond compared with those obtained from the Tersoff and Brenner EIPs using both the original and optimized parameter sets. For both the Tersoff and Brenner EIPs, the optimized parameter sets provide

TABLE IV. Lattice constant, cohesive energy, and acoustic-phonon velocities for in-plane graphite and diamond as given by the Tersoff and Brenner EIPs using original and optimized parameter sets as compared to experiment.

	Experiment	Tersoff original	Tersoff optimized	Brenner original	Brenner optimized
a_{lat} (Å) (gra)	2.459[a]	2.530	2.492	2.460	2.460
v_{TA} (m/s) (gra)	14920[b]	18274	14926	10641	12968
v_{LA} (m/s) (gra)	21819[b]	24002	21833	19388	20763
E_{coh} (eV) (gra)	−7.374 [c]	−7.396	−7.978	−7.395	−7.401
a_{lat} (Å) (dia)	3.567[d]	3.566	3.645	3.566	3.567
E_{coh} (eV) (dia)	−7.349 [c]	−7.371	−6.537	−7.370	−7.361

[a]Reference 53.
[b]From dispersion Ref. 51.
[c]Reference 54.
[d]Reference 55.

better agreement with acoustic-phonon velocities in graphite since these were included as fitting parameters. For the Tersoff EIP the optimized parameter set gives better agreement to the measured in-plane lattice constant of graphite but poorer agreement to the cohesive energy. For diamond, both the lattice constant and the cohesive energy are fit better by the original parameter set. For the Brenner EIP the optimized parameters leave the structural data for graphite and diamond unaltered due to the fitting procedure described above.

Recent calculations of the lattice thermal conductivity, κ_L, of SWCNTs based on a Boltzmann transport approach[23] have been performed with second- and third-order IFCs obtained from the Tersoff EIP with the original parameter set. Another recent molecular-dynamics simulation of κ_L (Ref. 24) employed the Brenner EIP with original parameters. Each calculation using these different transport models obtained values for κ_L that are inconsistently low compared to measured values.[8,56] For example, for SWCNTs with lengths around 3 μm and diameters in the 1–2 nm range, the measured room temperature κ_L's were around 3000–3500 W/m K. In contrast, calculated room temperature values for (10,10) SWCNTs were in both cases[23,24] considerably below 1000 W/m K. Employing the BTE approach developed previously by us,[23] we have calculated the κ_L for a 3 μm (10,10) SWCNT at $T=300$ K for each EIP using the original and optimized parameter sets. These values are listed in Table V. It is evident that for both Tersoff and Brenner EIPs, the optimized parameter sets give values of κ_L that are significantly larger and more consistent with those obtained experimentally. Part of the reason for this is that both potentials are too anharmonic as reflected in the third-order IFCs, so the phonon-phonon scattering rates are too large. It is interesting that the original Brenner parameters give extremely low κ_L and, in particular, much lower than even the original Tersoff parameters. This occurs because the corresponding TA and LA acoustic velocities are much too low, as seen in Table IV, and because κ_L depends on both phonon velocities and energies. To illustrate this sensitivity, we note that if the second-order IFCs from the optimized Brenner EIP are used with the third-order IFCs from the original parameter set, the resulting κ_L jumps from 250 to 1080 W/m K.

Room-temperature measurements of κ_L for suspended single-layer graphene (SLG) flakes with ~10 μm length along the transport direction have also been found to be around and above 3000 W/m K.[6,7] We have recently developed a BTE approach to calculate κ_L for suspended SLG and graphene supported on SiO_2 substrates.[17] In Table V, we include our calculated κ_L for a 10 μm length SLG using the original and optimized Tersoff and Brenner EIP parameters.[57] It is evident from the table that the values calculated using the optimized parameter sets once again are considerably closer to the measured values compared to the original sets. Like with the SWCNTs, this is due to improved representation of the acoustic-phonon dispersions and the anharmonic IFCs.

IV. SUMMARY AND CONCLUSIONS

Optimized parameter sets for the Tersoff and Brenner empirical interatomic potentials have been presented that provide overall improved agreement with the ZA, TA, and LA phonon branches in graphene and in-plane graphite. In particular, the near-zone-center velocities of these branches are better fit by the optimized parameter sets. These optimized parameters for the Tersoff and Brenner potentials have been demonstrated to improve the agreement between the calculated lattice thermal conductivity of SWCNTs and graphene and the corresponding measured values. Based on this, we expect that they will also provide better representations of the lattice dynamics and phonon thermal transport in other related systems such as graphene nanoribbons, multilayered graphene, and graphite.

TABLE V. Thermal conductivity of a 3 μm (10,10) SWCNT and a 10 μm suspended SLG flake at $T=300$ K using the original and optimized parameter sets for the Tersoff and Brenner EIPs.

	Original κ_L (W/m K)	Optimized κ_L (W/m K)
Tersoff SWCNT	600	1950
Brenner SWCNT	250	2000
Tersoff SLG	1900	3500
Brenner SLG	1100	3600

ACKNOWLEDGMENTS

The authors gratefully acknowledge the National Science Foundation under Grant No. CBET 0651381, and the Donors of the American Chemical Society Petroleum Research Fund for support of this research. We also wish to thank Natalio Mingo for his helpful input on this work.

[1] D. G. Onn, A. Witek, Y. Z. Qiu, T. R. Anthony, and W. F. Banholzer, Phys. Rev. Lett. **68**, 2806 (1992).
[2] J. R. Olson, R. O. Pohl, J. W. Vandersande, A. Zoltan, T. R. Anthony, and W. F. Banholzer, Phys. Rev. B **47**, 14850 (1993).
[3] L. Wei, P. K. Kuo, R. L. Thomas, T. R. Anthony, and W. F. Banholzer, Phys. Rev. Lett. **70**, 3764 (1993).
[4] G. A. Slack, Phys. Rev. **127**, 694 (1962).
[5] C. A. Klein and M. G. Holland, Phys. Rev. **136**, A575 (1964).
[6] A. A. Balandin, S. Ghosh, W. Bao, I. Calizo, D. Teweldebrhan, F. Miao, and C. Ning Lau, Nano Lett. **8**, 902 (2008).
[7] S. Ghosh, I. Calizo, D. Teweldebrhan, E. P. Pokatilov, D. L. Nika, A. A. Balandin, W. Bao, F. Miao, and C. N. Lau, Appl. Phys. Lett. **92**, 151911 (2008).
[8] C. Yu, L. Shi, Z. Yao, D. Li, and A. Majumdar, Nano Lett. **5**, 1842 (2005).
[9] E. Pop, D. Mann, Q. Wang, K. Goodson, and H. Dai, Nano Lett. **6**, 96 (2006).
[10] J. Che, T. Çağin, W. Deng, and W. Goddard III, J. Chem. Phys. **113**, 6888 (2000).
[11] A. Sparavigna, Phys. Rev. B **65**, 064305 (2002).
[12] A. Ward, D. A. Broido, D. A. Stewart, and G. Deinzer, Phys. Rev. B **80**, 125203 (2009).
[13] P. G. Klemens and D. F. Pedraza, Carbon **32**, 735 (1994).
[14] P. G. Klemens, J. Wide Bandgap Mater. **7**, 332 (2000).
[15] D. L. Nika, E. P. Pokatilov, A. S. Askerov, and A. A. Balandin, Phys. Rev. B **79**, 155413 (2009).
[16] D. L. Nika, S. Ghosh, E. P. Pokatilov, and A. A. Balandin, Appl. Phys. Lett. **94**, 203103 (2009).
[17] J. H. Seol, I. Jo, A. L. Moore, L. Lindsay, Z. H. Aitken, M. T. Pettes, X. Li, Z. Yao, R. Huang, D. A. Broido, N. Mingo, R. S. Ruoff, and L. Shi, Science **328**, 213 (2010).
[18] J. Hu, X. Ruan, and Y. P. Chen, Nano Lett. **9**, 2730 (2009).
[19] J. X. Cao, X. H. Yan, Y. Xiao, and J. W. Ding, Phys. Rev. B **69**, 073407 (2004).
[20] N. Mingo and D. A. Broido, Nano Lett. **5**, 1221 (2005).
[21] J. Wang and J.-S. Wang, Appl. Phys. Lett. **88**, 111909 (2006).
[22] Y. Gu and Y. Chen, Phys. Rev. B **76**, 134110 (2007).
[23] L. Lindsay, D. A. Broido, and N. Mingo, Phys. Rev. B **80**, 125407 (2009).
[24] J. A. Thomas, R. M. Iutzi, and A. J. H. McGaughey, Phys. Rev. B **81**, 045413 (2010).
[25] S. Berber, Y.-K. Kwon, and D. Tománek, Phys. Rev. Lett. **84**, 4613 (2000).
[26] J. Che, T. Çağin, and W. Goddard III, Nanotechnology **11**, 65 (2000).
[27] C. W. Padgett and D. W. Brenner, Nano Lett. **4**, 1051 (2004).
[28] Z. Yao, J.-S. Wang, B. Li, and G.-R. Liu, Phys. Rev. B **71**, 085417 (2005).
[29] D. Donadio and G. Galli, Phys. Rev. Lett. **99**, 255502 (2007).
[30] J. Lukes and H. Zhong, J. Heat Transfer **129**, 705 (2007).
[31] L. Wirtz and A. Rubio, Solid State Commun. **131**, 141 (2004).
[32] N. Mounet and N. Marzari, Phys. Rev. B **71**, 205214 (2005).
[33] O. Dubay and G. Kresse, Phys. Rev. B **67**, 035401 (2003).
[34] N. Bonini, M. Lazzeri, N. Marzari, and F. Mauri, Phys. Rev. Lett. **99**, 176802 (2007).
[35] N. Bonini, R. Rao, A. M. Rao, N. Marzari, and J. Menéndez, Phys. Status Solidi B **245**, 2149 (2008).
[36] S. Baroni *et al.* (unpublished), http://www.quantum-espresso.org
[37] G. Kresse *et al.* (unpublished), http://cms.mpi.univie.ac.at/vasp/
[38] X. Gonze *et al.* (unpublished), http://www.abinit.org/
[39] J. Tersoff, Phys. Rev. Lett. **61**, 2879 (1988).
[40] J. Tersoff, Phys. Rev. B **37**, 6991 (1988).
[41] D. W. Brenner, Phys. Rev. B **42**, 9458 (1990).
[42] D. W. Brenner, O. A. Shenderova, J. A. Harrison, S. J. Stuart, B. Mi, and S. B. Sinnott, J. Phys.: Condens. Matter **14**, 783 (2002).
[43] V. K. Tewary and B. Yang, Phys. Rev. B **79**, 075442 (2009).
[44] Q. Lu, M. Arroyo, and R. Huang, J. Phys. D **42**, 102002 (2009).
[45] W. H. Press, S. A. Teukolsky, W. T. Vetterling, and B. P. Flannery, *Numerical Recipes in Fortran* (Cambridge University Press, Cambridge, 1992).
[46] L. Lindsay and D. A. Broido, J. Phys.: Condens. Matter **20**, 165209 (2008).
[47] L. J. Porter, M. Yamaguchi, H. Kaburaki, and M. Tang, J. Appl. Phys. **81**, 96 (1997).
[48] D. A. Broido, A. Ward, and N. Mingo, Phys. Rev. B **72**, 014308 (2005).
[49] A. Y. Liu, M. L. Cohen, K. C. Hass, and M. A. Tamor, Phys. Rev. B **43**, 6742 (1991).
[50] J. Maultzsch, S. Reich, C. Thomsen, H. Requardt, and P. Ordejón, Phys. Rev. Lett. **92**, 075501 (2004).
[51] M. Mohr, J. Maultzsch, E. Dobardžić, S. Reich, I. Milošević, M. Damnjanović, A. Bosak, M. Krisch, and C. Thomsen, Phys. Rev. B **76**, 035439 (2007).
[52] J. H. Los, L. M. Ghiringhelli, E. J. Meijer, and A. Fasolino, Phys. Rev. B **72**, 214102 (2005).
[53] Y. Baskin and L. Meyer, Phys. Rev. **100**, 544 (1955).
[54] Compilation of L. Brewer, Lawrence Berkeley Laboratory Report No. LBL-3720 (unpublished).
[55] Y. S. Touloukian, R. K. Kirby, R. E. Taylor, and T. Y. R. Lee, *Thermophysical Properties of Matter* (Plenum, New York, 1977), Vol. 13.
[56] E. Pop, D. Mann, J. Cao, Q. Wang, K. Goodson, and H. Dai, Phys. Rev. Lett. **95**, 155505 (2005).
[57] In Ref. 17, the results for calculated thermal conductivity values for suspended SLG using the Tersoff EIP are slightly lower than the ones presented here because those results include phonon scattering by isotopic impurities.